Goshen College

Searching for cosmic strings using SPT-3G data

Ebtihal M. Abdelaziz*
(Dated: August 13, 2021)

I. INTRODUCTION

The South Pole Telescope (SPT) is a 10-meter microwave telescope that measures the cosmic microwave background (CMB) by repeatedly observing the same patch of the sky. SPT has a higher sensitivity to small scale features of the CMB and the B-mode (Divergence-free component of polarized CMB) anisotropy compared to Planck, a space-based CMB experiment. Planck has measured the CMB very precisely and tightly constrained the cosmological parameters of the ΛCDM model[1].SPT-3G is the newest camera that is currently collecting data on SPT. It has been running for 2.5 seasons of data [2]. SPT-3G has less noise levels compared to previous cameras used for SPT.

The CMB is an electromagnetic radiation that was emitted 380,000 years after the Big Bang making it the oldest observable light in the universe. It is studied using microwave telescopes such as SPT or satellites such as Planck. The data collected from telescopes can be used to create maps of CMB anisotropy. These maps show how the CMB light varies in temperature across the entire sky. The CMB light is also polarized, and maps of the polarization anisotropy can be constructed as well. Applying a Fourier Transform to the created maps results in the power spectra of the CMB. Precise measurement of the CMB power spectrum can be used to measure ΛCDM cosmological parameters, constrain a variety of models for physics beyond the standard model, and study astrophysical sources such as galaxy clusters and dusty high-redshift galaxies [2].

Cosmic strings are solutions of certain field theories, especially ones that are motivated by particle physics. They have not been detected before. The complex scalar field ϕ provides a simple example of field theories exhibiting string solutions [3]. The field ϕ can be described by the Lagrangian density

$$\mathcal{L} = \partial_\mu \phi^* \partial^\mu \phi - V(\phi), \quad V = \frac{1}{2}\lambda(|\phi|^2 - \frac{1}{2}\eta^2)^2. \tag{1}$$

This field has a global U(1) symmetry under the transformation $\phi \longrightarrow \phi e^{i\alpha}$ where α is a constant [4]. The Euler-Lagrange equation that follows from the previous equation (1) is

$$[\partial^2 + \lambda(|\phi|^2 - \frac{1}{2}\eta^2)]\phi = 0 \tag{2}$$

The ground state solution is $\phi = (\eta/\sqrt{2})\ exp((i)\alpha_0)$ where α_0 is a constant. This solution is stable, and it does not have a U(1) symmetry. This break in symmetry gives rise to string solutions.

In 2013, the Planck Collaboration published their constraints on Gμ, the string tension. The square of Gμ is directly proportional to the amplitude of the power spectrum of the string. Like the CMB, maps of anisotropy due to cosmic strings can be constructed following a certain string model. The power spectrum of the strings are obtained using Fourier Transform of these maps. This study aims to constrain Gμ using simulated primary CMB and cosmic strings power spectra and noise curves from SPT-3G. The motivation behind this study is to determine the sensitivity of SPT-3G to cosmic strings and compare that sensitivity to the results from Planck. Given that SPT-3G has a lower B-mode noise compared to Planck and is more sensitive to smaller angular resolutions, it seems that SPT-3G ought to be more sensitive to cosmic strings compared to Planck.

* ebtihal.muhammad2@gmail.com

II. METHODS

CAMB, a python package used to calculate the power spectrum of the primary CMB, was used to simulate the power spectrum of primary CMB obtained from SPT-3G [5]. CMBACT, a Fortran-based script that calculates the power spectrum of Nambu–Goto strings, was used to obtain the strings power spectrum [6]. CAMB allows the user to change the values of any cosmological parameter CAMB has and calculates the power spectrum accordingly. The power spectra obtained from CAMB and CMBACT are represented in FIG. 1.

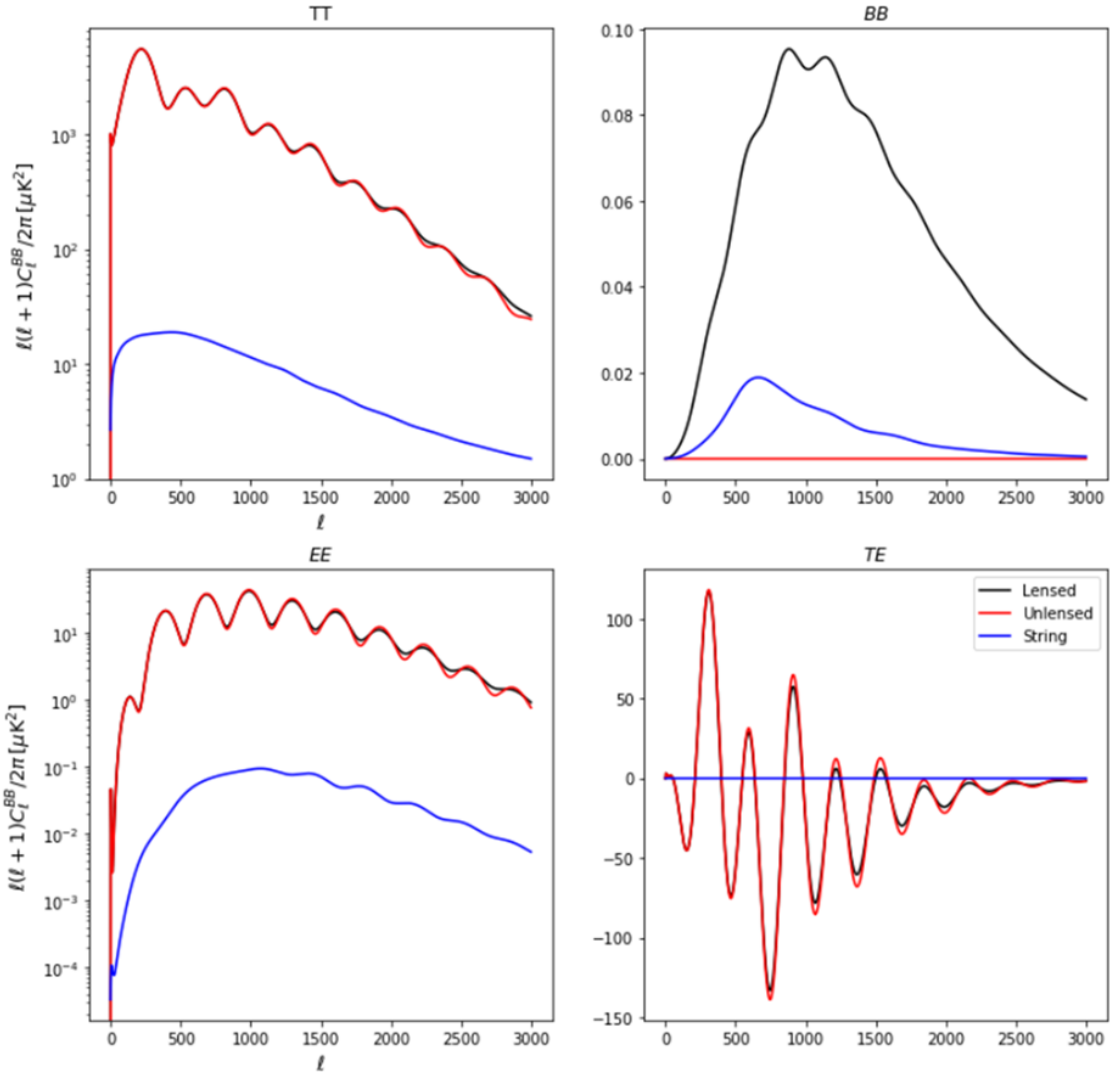

FIG. 1. The power spectra of the primary CMB and the cosmic strings obtained from CAMB and CMBACT respectively. The top right power spectrum is the temperature anisotropy power spectrum, the top left is the B-mode polarization power spectrum, the bottom right is the E-mode polarization power spectrum, the bottom left is the temperature-polarization power spectrum. The tensor to scalar ratio r was set to zero. Black is the primary CMB including gravitational lensing; red is the primary CMB without gravitational lensing; and blue is the cosmic string power spectrum.

CMBACT randomly generates a realization of the sky and calculates the power spectrum accordingly. For CMBACT to generate random, distinct realizations, the random seed had to have a negative value. Additionally, CMBACT has the property to average over different realizations of the string power spectrum. This can be done through changing the nexp value in the code to the number of realizations desired to be calculated and averaged over. We used this property to get the power spectrum resulting from the average of 120 different realizations. FIG. 2 shows different single-realization power spectra and the power spectrum averaged over 120 realizations.

The power spectra obtained from CMBACT and CAMB were used to forecast the uncertainties on Gμ using a

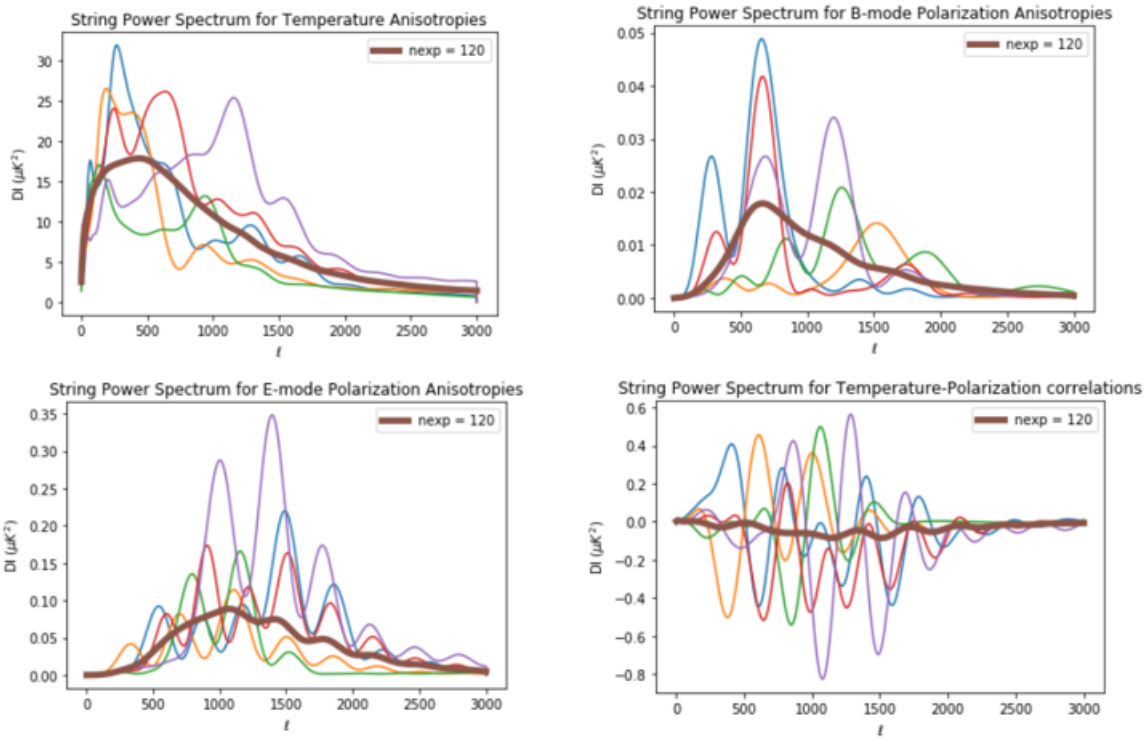

FIG. 2. The power spectra of 6 distinct cosmic string realizations and the average of 120 distinct cosmic string realizations (in dark brown) from CMBACT.

Fisher forecast. The Fisher forecast is a mathematical tool that calculates the maximum uncertainty on parameters without needing to do the full analysis. Its mathematical formalism is represented in the following equations.

$$F_{ij} = \sum_{\ell} \frac{2\ell+1}{2} f_{sky} \, \mathrm{Tr}\left(C_\ell^{-1}(\theta) \frac{\partial C_\ell}{\partial \theta_i} C_\ell^{-1}(\theta) \frac{\partial C_\ell}{\partial \theta_j} \right) \tag{3}$$

Where F is the Fisher matrix, ℓ is the multipole (or angular scale) of the anisotropies. f_{sky} is the observed sky fraction. C_ℓ^{-1} is the inverse of the C_ℓ matrix at fiducial (constant) values of the cosmological parameters. $\frac{\partial C_\ell}{\partial \theta_i}$ is the derivative of the C_ℓ matrix with respect to the ith cosmological parameter, and $\frac{\partial C_\ell}{\partial \theta_j}$ is the derivative of the C_ℓ matrix with respect to the jth cosmological parameter. Tr refers to the trace of the matrix. The C_ℓ matrix is represented in equation (4).

$$C_\ell \equiv \begin{pmatrix} C_\ell^{TT} + N_\ell^{TT} & C_\ell^{TE} & 0 \\ C_\ell^{TE} & C_\ell^{EE} + N_\ell^{EE} & 0 \\ 0 & 0 & C_\ell^{BB} + N_\ell^{BB} \end{pmatrix} \tag{4}$$

The derivatives of the C_ℓ matrix with respect to the ith cosmological parameter were calculated using the following procedure using CAMB. The C_ℓ matrix at fiducial values of the cosmological parameters was obtained, then the C_ℓ matrix evaluated at the same parameters except varying the ith parameter by 1% was calculated. The difference of the two C_ℓ matrices was divided by 1.01 times the fiducial value of the ith parameter, thus returning the derivative with respect to the ith parameter for every value of ℓ. The C_ℓ^{TT} is the result we obtain from the temperature power spectrum returned by CAMB plus the temperature power spectrum of the strings returned by CMBACT both divided by $\frac{2\pi}{\ell(\ell+1)}$.

The same can be said about the different elements of the C_ℓ matrix except they are the values of different power spectra. The C_ℓ^{TE} is the temperature-polarization correlation power spectrum; C_ℓ^{BB} is the B-mode (divergence-free

component of polarized CMB) power spectrum; and C_ℓ^{EE} is the E-mode (curl-free component of polarized CMB) power spectrum. N_ℓ^{TT} is the noise associated with the Temperature power spectrum, and the other N_ℓ terms are noise associated with other two polarization power spectra. The noise curves used are represented in the following FIG. 3. The uncertainties on the ith parameter σ_i are then calculated using equation (5).

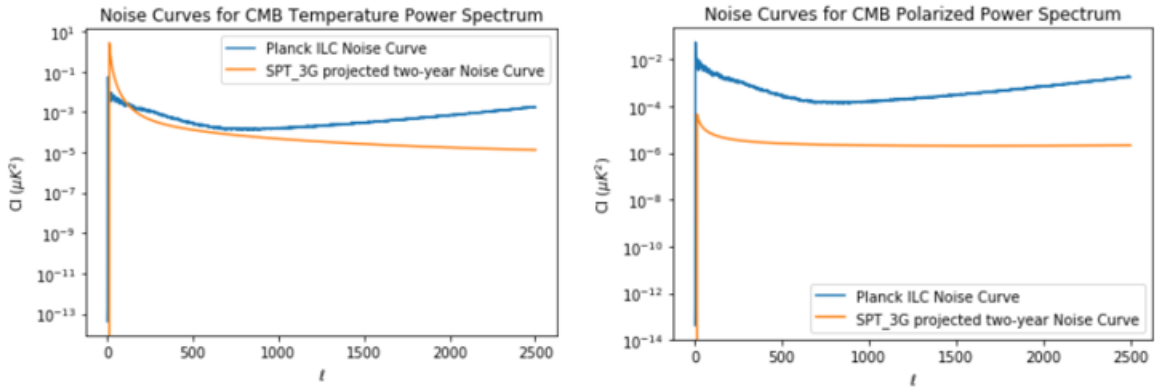

FIG. 3. The noise curves used for different forecasts. The left graph represents the temperature noise curves for both SPT-3G and Planck [7]. The right graph represents the polarization noise curves for both SPT-3G and Planck [7]. The temperature noise curves for SPT-3G are higher than the polarization noise levels since SPT-3G has more atmospheric noise in the temperature power spectrum compared to the polarization power spectrum.

$$\sigma_i \equiv \sigma(\theta_i) = \sqrt{(F_{ii}^{-1})} \tag{5}$$

The noise associated with the E-mode is considered to be approximately the same as the noise associated with the B-mode in all forecasts. We constructed a class representation of the Fisher forecast to easily calculate the uncertainties on cosmological parameters using different experimental configurations.

III. RESULTS

The Fisher forecast code was used to calculate the uncertainties on different cosmological parameters and Gμ. The following table shows the uncertainties found for each parameter for distinct configurations.

Forecasts							
Configuration	$\Omega_b h^2$	$\Omega_c h^2$	H_0	τ	n_s	$\log(A_s)$	Gμ
1st Configuration SPT,¬Gμ,¬BB	1.46E-4	2.03 $\times 10^{-3}$	7.68×10^{-1}	6.76 $\times 10^{-3}$	7.35 $\times 10^{-3}$	5.626×10^{-3}	-
2ed Configuration SPT,¬BB	1.49×10^{-4}	2.13×10^{-3}	8.01×10^{-1}	6.78×10^{-3}	7.43×10^{-3}	5.80×10^{-3}	1.12×10^{-8}
3rd Configuration SPT,¬TT,¬TE	1.57×10^{-3}	6.43×10^{-3}	3.31	6.98×10^{-3}	2.17×10^{-2}	1.01×10^{-2}	2.69×10^{-8}
4th Configuration SPT	1.44×10^{-4}	1.8×10^{-3}	6.71×10^{-1}	6.78×10^{-3}	6.7×10^{-3}	5.62×10^{-3}	8.37×10^{-9}
5th Configuration Planck	1.12×10^{-4}	1.37×10^{-3}	5.51×10^{-1}	6.77×10^{-3}	4.11×10^{-3}	6.09×10^{-3}	1.92×10^{-8}
6th Configuration SPT and Planck	7.84×10^{-5}	1.05×10^{-3}	4.07×10^{-1}	4.7×10^{-3}	3.13×10^{-3}	4.01×10^{-3}	6.59×10^{-9}

Table 1. The table shows the uncertainties obtained by using the Fisher forecast code on the ΛCDM cosmological parameters and the string tension Gμ The first four configurations are done using SPT-3G data, hence the SPT label. The fifth is done using Planck data. The sixth configuration is the combination of SPT-3G and Planck data. ¬ refers to the exclusion of power spectra or parameters from either the C_ℓ matrix of the Fisher matrix.

The first configuration was done to test the code by calculating the uncertainties on the ΛCDM cosmological parameters. This allowed us to compare the resulted constraints to previously published work. The numbers were close to previous forecasts. The ℓ_{max} was set to 3000, and the ℓ_{min} was set to 100. The Lensed primary CMB power spectrum was used as well. A τ prior was used given that most of the information needed to define tau are at low angular scale. We were not using low angular scale data since SPT does not resolve objects with angular scale below 100 very well. The B-mode power spectrum information were not included in the C_ℓ matrix for the first configuration. The string tension Gμ was not part of the parameters that were included in the Fisher matrix for the first configuration. Also, f_{sky} was set to the fraction of the sky observed by SPT-3G which is about 3.5 percent. The second configuration had the same conditions as the first configuration except that we added the string tension Gμ to the Fisher matrix. The value of Gμ used is $G\mu = 1 \times 10^{-7}$. The third configuration had similar setup to the second configuration. Nevertheless, the third configuration did not include the TT and TE spectra but included the BB spectrum. The fourth configuration had the same experimental assumptions as the first one, except the fisher matrix includes Gμ and the C_ℓ matrix included information from all power spectra. This means the fourth configuration has all the possible information we get from CAMB, so we expect it to produce the least uncertainty.

The fifth configuration shows the uncertainty obtained when using the Fisher Forecast code with Planck data and noise levels. Compared to the published Planck results, the uncertainties in the table are lower. This could be due to the Fisher Forecast returning lower uncertainties compared to other analysis techniques. Also, the uncertainty reported here is the 1-sigma uncertainty while the published Planck result is the upper limit at 95% UL. The fifth forecast did not include the BB spectrum, since Planck did not report them in the published results. It should be noted that the fourth configuration shows less uncertainties in Gμ compared to the fifth configuration. Thus, this shows that SPT-3G can provide better constraints on Gμ compared to Planck. The sixth forecast was computed by adding the two fisher matrices: from the fourth configuration and from the fifth configuration. This configuration has the best uncertainties given the complementary data collected by SPT and Planck. SPT has high resolution of the B-mode power spectrum, and Planck has a high resolution of the temperature power spectrum.

In addition to the table above, a distribution of the different string realizations and the associated uncertainties were obtained using CMBACT. The nexp was set to 1 and the random seed in the code was adjusted so that it depends on the clock. This means when the code was run, the seed was automatically updated, and we got a different realization. The distribution of the uncertainties of different string realizations was found using 200 distinct realizations. The following figure (FIG. 4) represents the found string uncertainty distribution.

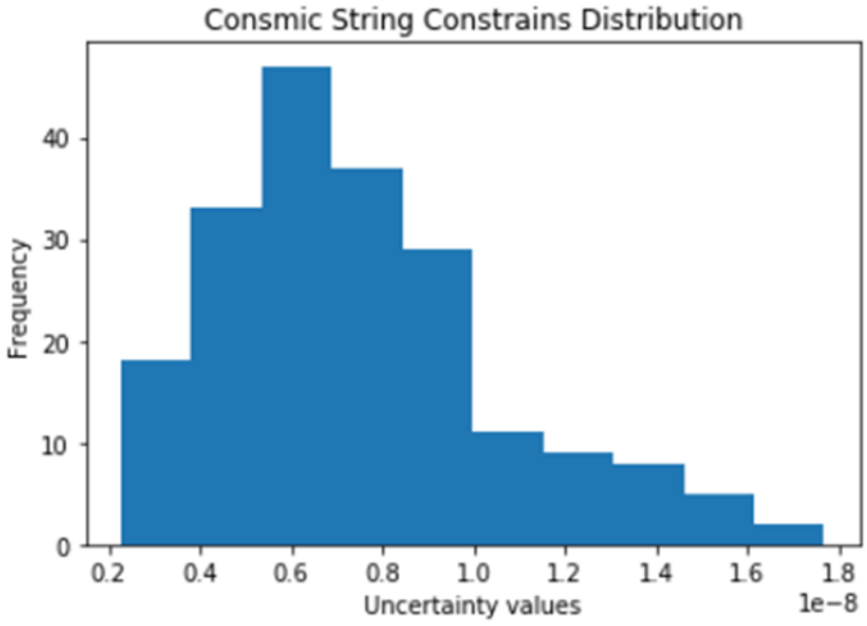

FIG. 4. The uncertainty distribution of the cosmic strings using 200 distinct string realizations.

The distribution shows that most realizations would give us uncertainties close to the string uncertainties reported

in the fourth configuration. The standard deviation of this distribution is 3.14×10^{-9}. The effect of increasing the observed sky fraction on the uncertainty of the string can be seen in FIG. 5.

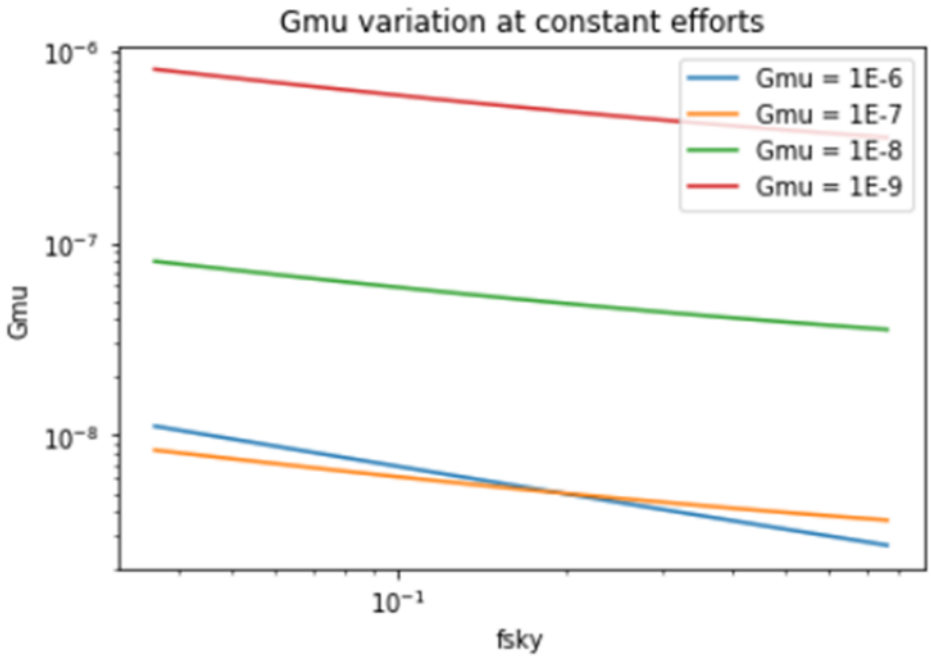

FIG. 5. The effect of increasing the observed sky fraction by SPT at constant experimental efforts on the uncertainty of the string tension.

As shown in the figure, it seems that increasing the observed sky fraction by SPT increases the reported uncertainties regardless of the initial value of the string tension.

IV. CONCLUSION

The Fisher forecast shows that SPT is more sensitive than Planck in terms of constraining the string tension. Combining both Planck and SPT data yields the best constraints on the string tension and all other ΛCDM cosmological parameters. These results are shown by the uncertainties reported in the configuration table. These results agree with our initial thoughts given SPT-3G resolution for small angular scales and its low B-mode polarization power spectrum noise levels and Planck low-noise temperature power spectrum.

Since CMB-S4 is going to have improved noise levels for polarized CMB maps and high resolution for low angular scale, it is possible that CMB-S4 can constrain $G\mu$ better than SPT-3G [8]. This is especially true since CMB-S4 is going to observe about 40 percent of the sky and our results show that increasing the sky fraction at SPT-3G resolution and noise levels reduces the uncertainty on $G\mu$ [8].

[1] P. A. R. Ade, N. Aghanim, C. Armitage-Caplan, M. Arnaud, M. Ashdown, F. Atrio-Barandela, J. Aumont, C. Baccigalupi, A. J. Banday, and et al., Astronomy Astrophysics **571**, A25 (2014).

[2] L. Balkenhol, D. Dutcher, P. A. R. Ade, Z. Ahmed, E. Anderes, A. J. Anderson, M. Archipley, J. S. Avva, K. Aylor, P. S. Barry, R. B. Thakur, K. Benabed, A. N. Bender, B. A. Benson, F. Bianchini, L. E. Bleem, F. R. Bouchet, L. Bryant, K. Byrum, J. E. Carlstrom, F. W. Carter, T. W. Cecil, C. L. Chang, P. Chaubal, G. Chen, H. M. Cho, T. L. Chou, J. F. Cliche, T. M. Crawford, A. Cukierman, C. Daley, T. de Haan, E. V. Denison, K. Dibert, J. Ding, M. A. Dobbs, W. Everett, C. Feng, K. R. Ferguson, A. Foster, J. Fu, S. Galli, A. E. Gambrel, R. W. Gardner, N. Goeckner-Wald, R. Gualtieri, S. Guns, N. Gupta, R. Guyser, N. W. Halverson, A. H. Harke-Hosemann, N. L. Harrington, J. W. Henning, G. C. Hilton, E. Hivon, G. P. Holder, W. L. Holzapfel, J. C. Hood, D. Howe, N. Huang, K. D. Irwin, O. B. Jeong, M. Jonas, A. Jones, T. S. Khaire, L. Knox, A. M. Kofman, M. Korman, D. L. Kubik, S. Kuhlmann, C. L. Kuo, A. T. Lee, E. M. Leitch, A. E. Lowitz, C. Lu, S. S. Meyer, D. Michalik, M. Millea, J. Montgomery, A. Nadolski, T. Natoli, H. Nguyen, G. I. Noble, V. Novosad, Y. Omori, S. Padin, Z. Pan, P. Paschos, J. Pearson, C. M. Posada, K. Prabhu, W. Quan, A. Rahlin,

C. L. Reichardt, D. Riebel, B. Riedel, M. Rouble, J. E. Ruhl, J. T. Sayre, E. Schiappucci, E. Shirokoff, G. Smecher, J. A. Sobrin, A. A. Stark, J. Stephen, K. T. Story, A. Suzuki, K. L. Thompson, B. Thorne, C. Tucker, C. Umilta, L. R. Vale, K. Vanderlinde, J. D. Vieira, G. Wang, N. Whitehorn, W. L. K. Wu, V. Yefremenko, K. W. Yoon, and M. R. Young, (2021), arXiv:2103.13618 [astro-ph.CO].

[3] T. Vachaspati, L. Pogosian, and D. Steer, Scholarpedia **10**, 31682 (2015).

[4] M. B. Hindmarsh and T. W. B. Kibble, Reports on Progress in Physics **58**, 477–562 (1995).

[5] A. Lewis, A. Challinor, and A. Lasenby, The Astrophysical Journal **538**, 473–476 (2000).

[6] L. Pogosian and T. Vachaspati, Physical Review D **60** (1999), 10.1103/physrevd.60.083504.

[7] S. Raghunathan, private communication.

[8] K. Abazajian, G. Addison, P. Adshead, Z. Ahmed, S. W. Allen, D. Alonso, M. Alvarez, A. Anderson, K. S. Arnold, C. Baccigalupi, K. Bailey, D. Barkats, D. Barron, P. S. Barry, J. G. Bartlett, R. B. Thakur, N. Battaglia, E. Baxter, R. Bean, C. Bebek, A. N. Bender, B. A. Benson, E. Berger, S. Bhimani, C. A. Bischoff, L. Bleem, S. Bocquet, K. Boddy, M. Bonato, J. R. Bond, J. Borrill, F. R. Bouchet, M. L. Brown, S. Bryan, B. Burkhart, V. Buza, K. Byrum, E. Calabrese, V. Calafut, R. Caldwell, J. E. Carlstrom, J. Carron, T. Cecil, A. Challinor, C. L. Chang, Y. Chinone, H.-M. S. Cho, A. Cooray, T. M. Crawford, A. Crites, A. Cukierman, F.-Y. Cyr-Racine, T. de Haan, G. de Zotti, J. Delabrouille, M. Demarteau, M. Devlin, E. D. Valentino, M. Dobbs, S. Duff, A. Duivenvoorden, C. Dvorkin, W. Edwards, J. Eimer, J. Errard, T. Essinger-Hileman, G. Fabbian, C. Feng, S. Ferraro, J. P. Filippini, R. Flauger, B. Flaugher, A. A. Fraisse, A. Frolov, N. Galitzki, S. Galli, K. Ganga, M. Gerbino, M. Gilchriese, V. Gluscevic, D. Green, D. Grin, E. Grohs, R. Gualtieri, V. Guarino, J. E. Gudmundsson, S. Habib, G. Haller, M. Halpern, N. W. Halverson, S. Hanany, K. Harrington, M. Hasegawa, M. Hasselfield, M. Hazumi, K. Heitmann, S. Henderson, J. W. Henning, J. C. Hill, R. Hlozek, G. Holder, W. Holzapfel, J. Hubmayr, K. M. Huffenberger, M. Huffer, H. Hui, K. Irwin, B. R. Johnson, D. Johnstone, W. C. Jones, K. Karkare, N. Katayama, J. Kerby, S. Kernovsky, R. Keskitalo, T. Kisner, L. Knox, A. Kosowsky, J. Kovac, E. D. Kovetz, S. Kuhlmann, C. lin Kuo, N. Kurita, A. Kusaka, A. Lahteenmaki, C. R. Lawrence, A. T. Lee, A. Lewis, D. Li, E. Linder, M. Loverde, A. Lowitz, M. S. Madhavacheril, A. Mantz, F. Matsuda, P. Mauskopf, J. McMahon, M. McQuinn, P. D. Meerburg, J.-B. Melin, J. Meyers, M. Millea, J. Mohr, L. Moncelsi, T. Mroczkowski, S. Mukherjee, M. Münchmeyer, D. Nagai, J. Nagy, T. Namikawa, F. Nati, T. Natoli, M. Negrello, L. Newburgh, M. D. Niemack, H. Nishino, M. Nordby, V. Novosad, P. O'Connor, G. Obied, S. Padin, S. Pandey, B. Partridge, E. Pierpaoli, L. Pogosian, C. Pryke, G. Puglisi, B. Racine, S. Raghunathan, A. Rahlin, S. Rajagopalan, M. Raveri, M. Reichanadter, C. L. Reichardt, M. Remazeilles, G. Rocha, N. A. Roe, A. Roy, J. Ruhl, M. Salatino, B. Saliwanchik, E. Schaan, A. Schillaci, M. M. Schmittfull, D. Scott, N. Sehgal, S. Shandera, C. Sheehy, B. D. Sherwin, E. Shirokoff, S. M. Simon, A. Slosar, R. Somerville, D. Spergel, S. T. Staggs, A. Stark, R. Stompor, K. T. Story, C. Stoughton, A. Suzuki, O. Tajima, G. P. Teply, K. Thompson, P. Timbie, M. Tomasi, J. I. Treu, M. Tristram, G. Tucker, C. Umiltà, A. van Engelen, J. D. Vieira, A. G. Vieregg, M. Vogelsberger, G. Wang, S. Watson, M. White, N. Whitehorn, E. J. Wollack, W. L. K. Wu, Z. Xu, S. Yasini, J. Yeck, K. W. Yoon, E. Young, and A. Zonca, (2019), arXiv:1907.04473 [astro-ph.IM].